Transcutaneous carbon dioxide suppresses skeletal muscle atrophy in a mouse model of oral squamous cell carcinoma

Sasaki, Aki ; Takeda, Daisuke ; Kawai, Hotaka ; Tadokoro, Yoshiaki ; Murakami, Aki ; Yatagai, Nanae ; Arimoto, Satomi ; Nagatsuka, Hitoshi ⋯

(Citation)
PLoS ONE,19(4):e0302194

(Issue Date)
2024-04-17

(Resource Type)
journal article

(Version)
Version of Record

(URL)
https://hdl.handle.net/20.500.14094/0100489726

PLOS ONE

RESEARCH ARTICLE

Transcutaneous carbon dioxide suppresses skeletal muscle atrophy in a mouse model of oral squamous cell carcinoma

Aki Sasaki[1☯], Daisuke Takeda[1☯], Hotaka Kawai[2☯], Yoshiaki Tadokoro[1], Aki Murakami[1], Nanae Yatagai[1], Satomi Arimoto[1], Hitoshi Nagatsuka[2], Masaya Akashi[1], Takumi Hasegawa[1]*

1 Department of Oral Maxillofacial Surgery, Kobe University Graduate School of Medicine, Japan, **2** Department of Oral Pathology and Medicine, Graduate School of Medicine, Dentistry and Pharmaceutical Sciences, Okayama University, Okayama, Japan

☯ These authors contributed equally to this work.
* hasetaku@med.kobe-u.ac.jp

OPEN ACCESS

Citation: Sasaki A, Takeda D, Kawai H, Tadokoro Y, Murakami A, Yatagai N, et al. (2024) Transcutaneous carbon dioxide suppresses skeletal muscle atrophy in a mouse model of oral squamous cell carcinoma. PLoS ONE 19(4): e0302194. https://doi.org/10.1371/journal.pone.0302194

Editor: Agustín Guerrero-Hernandez, Cinvestav-IPN, MEXICO

Received: November 27, 2023

Accepted: March 30, 2024

Published: April 17, 2024

Data Availability Statement: All relevant data are within the manuscript and its Supporting information files.

Funding: JSPS KAKENHI (grant number 20K18724).

Competing interests: The authors have declared that no competing interests exist.

Abstract

Cancer cachexia causes skeletal muscle atrophy, impacting the treatment and prognosis of patients with advanced cancer, but no treatment has yet been established to control cancer cachexia. We demonstrated that transcutaneous application of carbon dioxide (CO_2) could improve local blood flow and reduce skeletal muscle atrophy in a fracture model. However, the effects of transcutaneous application of CO_2 in cancer-bearing conditions are not yet known. In this study, we calculated fat-free body mass (FFM), defined as the skeletal muscle mass, and evaluated the expression of muscle atrophy markers and uncoupling protein markers as well as the cross-sectional area (CSA) to investigate whether transcutaneous application of CO_2 to skeletal muscle could suppress skeletal muscle atrophy in cancer-bearing mice. Human oral squamous cell carcinoma was transplanted subcutaneously into the upper dorsal region of nude mice, and 1 week later, CO_2 gas was applied to the legs twice a week for 4 weeks and FFM was calculated by bioimpedance spectroscopy. After the experiment concluded, the quadriceps were extracted, and muscle atrophy markers (muscle atrophy F-box protein (MAFbx), muscle RING-finger protein 1 (MuRF-1)) and uncoupling protein markers (uncoupling protein 2 (UCP2) and uncoupling protein 3 (UCP3)) were evaluated by real-time polymerase chain reaction and immunohistochemical staining, and CSA by hematoxylin and eosin staining. The CO_2-treated group exhibited significant mRNA and protein expression inhibition of the four markers. Furthermore, immunohistochemical staining showed decreased MAFbx, MuRF-1, UCP2, and UCP3 in the CO_2-treated group. In fact, the CSA in hematoxylin and eosin staining and the FFM revealed significant suppression of skeletal muscle atrophy in the CO_2-treated group. We suggest that transcutaneous application of CO_2 to skeletal muscle suppresses skeletal muscle atrophy in a mouse model of oral squamous cell carcinoma.

Introduction

Cancer cachexia is a multifactorial syndrome defined by an ongoing loss of skeletal muscle mass (with or without loss of fat mass) that cannot be fully reversed by conventional nutritional support and leads to progressive functional impairment. Its pathophysiology is characterized by a negative protein and energy balance driven by a variable combination of reduced food intake and abnormal metabolism [1, 2]. Cancer cachexia has been defined in various ways, but the most prominent characteristic is skeletal muscle atrophy. Cancer cachexia is quite common in patients with advanced cancer [3, 4]. Furthermore, it is a cause of resistance to chemotherapy and radiotherapy and is attributed to at least 20% of deaths in cancer patients [5, 6]. However, there is currently no established treatment for cancer cachexia, and skeletal muscle atrophy is the most significant clinical symptom [3, 5].

Skeletal muscle mass is maintained by a balance between protein synthesis and proteolysis, and if this balance shifts to a catabolic state, it leads to skeletal muscle atrophy [6]. Skeletal muscle atrophy is regulated by the ubiquitin–proteasome pathway, specifically the rate-limiting enzymes of MAFbx (muscle atrophy F-box protein) and MuRF-1 (muscle RING-finger protein 1). Furthermore, several in vivo studies suggested that these factors are increased due to skeletal muscle atrophy [7–11].

Skeletal muscle atrophy is also related to a decrease in ATP synthesis. This is thought to be regulated by uncoupling proteins (UCPs), which are recognized as transporters of proton ions between the mitochondrial inner membrane and the mitochondrial matrix. There are five known isoforms of UCP (UCP1 to UCP5). UCP2 is present in all tissues, including skeletal muscle, while UCP3 is expressed in skeletal and cardiac muscle [12]. Several in vivo studies suggested that UCP2 and UCP3 are related to skeletal muscle atrophy [12–15].

Carbon dioxide (CO_2) therapy is widely known as an effective treatment to improve blood flow and has been indicated for various diseases such as heart disease and skin conditions [16]. We demonstrated that transcutaneous application of CO_2 could improve local blood flow and promote the suppression of muscle atrophy and contraction, as well as the recovery of muscle damage [17–23]. However, while we have demonstrated the effect of transcutaneous application of CO_2 in suppressing tumor growth [24], we have not demonstrated the effect of cancer cachexia. Therefore, we hypothesized that transcutaneous CO_2 application suppresses skeletal muscle atrophy in oral cancer-bearing mice. In this study, we investigated the relationship of skeletal muscle mass and the expression of MAFbx, MuRF-1, UCP2, and UCP3 in the CO_2-treated group.

Materials and methods

Cell culture

In this study, we obtained an oral cancer cell line, HSC-3, from the Health Science Research Resources Bank (Osaka, Japan). This cell line originates from a metastatic deposit of a poorly differentiated squamous cell carcinoma (SCC) of the tongue, specifically in a mid-internal jugular lymph node, extracted from a 64-year-old man. The cultivation of HSC-3 cells was performed using Eagle's minimum essential medium (Sigma–Aldrich, St. Louis, MO, USA), which was supplemented with fetal bovine serum (10%; Thermo Fisher Scientific, Waltham, MA, USA), as well as a solution of penicillin and streptomycin (1000 units/mL; Sigma–Aldrich). Trypsin (0.25%; FUJIFILM Wako Pure Chemical Corporation, Osaka, Japan) and ethylenediaminetetraacetic acid (0.02%; DOJINDO LABORATORIES, Kumamoto, Japan) solutions were used to isolate cells for subculture, as previously described [24].

Animal models

We obtained 7-week-old male athymic BALB/cAJcl–nu/nu nude mice from CLEA Japan (Tokyo, Japan). These mice were maintained in a pathogen-free environment by trained staff, strictly adhering to institutional protocols. The animal experiments were approved by the Institutional Animal Care and Use Committee (permission number: P-210105) and were performed in accordance with the Guidelines for Animal Experimentation at Kobe University Animal Experimentation Regulations. We injected HSC-3 cells (2.0×10^6 cells in 500 μL Eagle's minimum essential medium per mouse) subcutaneously into the upper dorsal region of the mouse under anesthesia using isoflurane, in accordance with previous studies of animal models of cancer cachexia [25–28].

Measurement of fat-free body mass by bioimpedance spectroscopy

In vivo body composition was measured by bioimpedance spectroscopy (ImpediVet; ImpediMed, Carlsbad, CA, USA) once a week for 4 weeks. The mice underwent weighing, followed by anesthesia induction using a mixed anesthetic solution comprising medetomidine, midazolam, and butorphanol. The anesthesia was administered through intraperitoneal injection, after which the mice were positioned in a prone stance on a table. Four 25G needles, functioning as electrodes, were positioned subcutaneously along the midline of the back in accordance with the instructions provided by the manufacturer. The total body water was quantified and utilizing the differing water composition of adipose and lean tissues, an approximation of the overall fat mass and fat-free body mass (FFM) was calculated. The skeletal muscle mass was defined as the FFM. FFM (kg) was calculated every week starting from the tumor transplantation day until the end of the experiment. During each measurement, we calculated the percentage of FFM relative to the individual's body weight and tracked its changes over time, using the day of tumor transplantation as the reference point.

Transcutaneous CO_2 treatment

The skin surface of the legs, excluding the tumor implant site, was covered with a CO_2 absorption-enhancing hydrogel (CO_2 hydrogel) obtained from CO_2 Tech (Kobe, Japan). This area was sealed with a polyethylene bag to retain the gas inside (Fig 1). Then 100% CO_2 gas was pumped into the bag and transcutaneous CO_2 treatment was applied for 20 min. Upon completion of the CO_2 treatment duration, the CO_2 hydrogel was gently removed from the treated area. Control animals were treated similarly, with room air replacing the CO_2 [18, 23, 24].

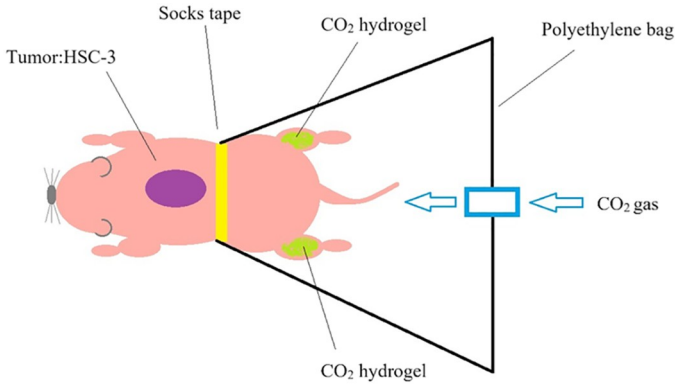

Fig 1. Transcutaneous CO_2 treatment.

https://doi.org/10.1371/journal.pone.0302194.g001

The skin surface of the legs, excluding the tumor implant site, was covered with a CO_2 absorption-enhancing hydrogel (CO_2 hydrogel). 100% CO_2 gas was pumped into the bag and transcutaneous CO_2 treatment was applied for 20 min.

In vivo

Fourteen mice were randomly assigned to two groups: a CO_2-treated group (n = 7) and a control group (n = 7). The treatment was initiated at 7 days following the implantation of HSC-3 cells and was administered twice a week for 4 weeks. Referring to our previous studies, the endpoint was set at 4 weeks after implantation [24]. Tumor volume was calculated as previously described according to the formula $V = \pi/6 \times a^2 \times b$, where a and b represent the shorter and longer diameters of the tumor, respectively [24].

Surgical procedure

The treatment protocol spanned a duration of 4 weeks from its initiation, and upon its completion, 24 hours after the final treatment session, the mice were humanely sacrificed under anesthesia. No animals died before euthanization. Mice were adequately anesthetized by inhalation with isoflurane and compassionately killed by decapitation to remove blood. Subsequently, both the tumor and bilateral quadriceps muscles were extracted, and we harvested the bilateral quadriceps muscles from mice. One was used for the RNA extraction, and the other was used for hematoxylin and eosin (H&E) and immunohistochemical (IHC) staining.

Quantitative real-time polymerase chain reaction

To analyze the mRNA expression levels of *MAFbx*, *MuRF-1*, *UCP2*, and *UCP3* in the quadriceps muscles of both the control and CO_2-treated groups, quantitative real-time PCR was employed. The treated quadriceps muscles for quantitative real-time PCR were processed for total RNA extraction according to the manufacturer's guidelines using a RNeasy Mini Kit (Qiagen, Valencia, CA, USA), which involves selective binding to a silica gel-based membrane [24]. cDNA was synthesized from a total of 300 ng RNA using the High-Capacity cDNA Transcription kit from Applied Biosystems (Foster City, CA, USA). The quantification of mRNA transcripts was executed using the Applied Biosystems StepOne Real-Time PCR System (Applied Biosystems). Real-Time PCR reactions (20 μL) contained 0.5 μM forward primer, 0.5 μM reverse primer, and 1 μL cDNA template from the RT reaction, and 10 μL (2×) Power SYBR green master mix (Applied Biosystems). Reaction conditions were 95˚C for 10 min, followed by 40 cycles of 95˚C for 15 sec and 60˚C for 1 min. The level of each target gene was normalized to *ACTB* levels and expressed relative to the levels of the control group ($^{\Delta\Delta}$CT method; Applied Biosystems) [19, 24]. The primer sequences purchased from Thermo Fisher Scientific are described in Table 1 [10].

Table 1. Specific primer sequences for real-time polymerase chain reaction analysis.

Gene name	Primer sequence (5'-3')	
ACTB	Fw: CTG GCT CCT AGC ACC ATG AA	Rv: CTG CTT GCT GAT CCA CAT CT
MAFbx	Fw: TTA TGC ACG CTG GTC CAG A	Rv: TGT AAG CAC ACA GGC AGG TC
MuRF-1	Fw: GGT GCC TAC TTG CTC CTT GT	Rv: TCA CCT GG TGG CTG TTT TC
UCP2	Fw: TGT AAG CAC ACA GGC AGG TC	Rv: CAT GGT CAG GGC ACA GTG GC
UCP3	Fw: GTG ACC TAT GAC ATC ATC AAG GA	Rv: GCT CCA AAG GCA GAG ACA AAG

https://doi.org/10.1371/journal.pone.0302194.t001

Hematoxylin and eosin (H&E) staining and analysis of the cross-sectional area of muscle

The quadriceps muscles were treated for H&E staining without detaching from the femur, to use the femur the referencing the gross position, by fixation in 4% paraformaldehyde and embedding in paraffin wax. We generated a 3-μm-thick section of the quadriceps muscle with the midpoint of the femur using a microtome and stained with H&E. The cross-sectional area of the muscle was compared between groups. Section images were captured randomly using a BZ-X700 microscope at ×400 magnification (KEYENCE, Osaka, Japan) and the cross-sectional area was measured using a BZ-X700 Analyzer (KEYENCE) [18].

Immunohistochemical staining (IHC) and quantification of protein expression

IHC was performed using the antibodies outlined in Table 2. The sections were subjected to deparaffinization using a series of xylene treatments lasting 15 min each, followed by rehydration through graded ethanol solutions. Endogenous peroxidase activity was blocked by incubating the sections in a solution of 0.3% H_2O_2 in methanol for a duration of 30 min. Subsequent to antigen retrieval, the sections were subjected to treatment with 10% normal serum for 15 min, followed by incubation with primary antibodies overnight at a temperature of 4˚C. The signals were amplified using the avidin–biotin complex method (Vector Lab, Burlingame, CA, USA). Color development was achieved using DAB (Nakalai Tesque, Kyoto, Japan), and the sections were counterstained with Mayer's hematoxylin. The staining outcomes were visualized using an all-in-one fluorescence microscope (BZ-X700; KEYENCE) [19]. Three locations were arbitrarily selected from one sample at ×400 magnification and the immunohistochemical staining ratio of muscle fibers that were judged DAB positive was quantified. The same work was performed for all samples and the average value was calculated for each sample.

Statistical analysis

Data are presented as the average ±standard deviation. EXCEL Toukei Ver. 7.0 for Windows (ESUMI Co., Ltd., Tokyo, Japan) was used for the statistical analyses performed on the data for two groups by the Mann–Whitney U test. The level of statistical significance was set at $P<0.05$.

Results

1. FFM (defined as the skeletal muscle mass)

At 7 days after HSC-3 implantation, CO_2 gas was applied to the legs twice a week for 4 weeks. We investigated the changes in FFM over time relative to the baseline at the beginning of the

Table 2. Primary antibodies used in IHC.

Primary antibody	Immunized animal	Antigen retrieval	Dilution	Supplier
MAFbx	Mouse	microwave heating in Dako Target Retrieval Solution, pH9(×10) at 100˚C for three and a half minutes	1:1200	ProteinTech Group, Chicago, IL
MuRF-1	Rabbit	microwave heating in Dako Target Retrieval Solution, pH9(×10) at 100˚C for three and a half minutes	1:500	ProteinTech Group, Chicago, IL
UCP2	Rabbit	microwave heating in Dako Target Retrieval Solution, pH9(×10) at 100˚C for three and a half minutes	1:400	Bioss Antibodies, Boston, MA, United States
UCP3	Rabbit	microwave heating in Dako Target Retrieval Solution, pH9(×10) at 100˚C for three and a half minutes	1:200	Novus Biologicals LLC, Centennial, Colorado, United States

https://doi.org/10.1371/journal.pone.0302194.t002

measurement. At the end of the experiment, FFM (average ± standard deviation) of the CO_2-treated group was 1.11± 0.15, and that of the control group was 0.94 ± 0.10. Furthermore, FFM had decreased by significantly more in the control group than in the CO_2-treated group (*P<0.05) (Fig 2).

2. Tumor volume

At any point during the measurement of tumor volume, the differences in the tumor volume were not statistically significant in the control and CO_2-treated groups (Fig 3).

3. Gene expression

At the end of the experiment, quantitative real-time PCR demonstrated that the mRNA expression levels of *MAFbx*, *MuRF-1*, *UCP2*, and *UCP3* were significantly suppressed in the CO_2-treated group compared with the control group (*P<0.05, **P<0.01) (Fig 4). At the end of the experiment, average *MAFbx* expression levels (± standard deviation) in the control group were 1.00±0.66, and those in the CO_2-treated group were 0.41±0.11. *MuRF-1* expression levels in the control group were 1.00±0.51, and those in the CO_2-treated group were 0.32±0.21. *UCP2* expression levels in the control group were 1.00±0.82, and those in the CO_2-treated group were 0.27±0.17. *UCP3* expression levels in the control group were 1.00±0.18, and those in the CO_2-treated group were 0.70±0.23.

At the end of the experiment, average *MAFbx* expression levels (± standard deviation) in the control group were 1.00±0.66, and those in the CO_2-treated group were 0.41±0.11. *MuRF-1* expression levels in the control group were 1.00±0.51, and those in the CO_2-treated group were 0.32±0.21. *UCP2* expression levels in the control group were 1.00±0.82, and those in the CO_2-treated group were 0.27±0.17. *UCP3* expression levels in the control group were 1.00 ±0.18, and those in the CO_2-treated group were 0.70±0.23.

4. Histological analysis

At the end of the experiment, immunohistochemical staining showed significantly lower expression of MAFbx, MuRF-1, UCP2, and UCP3 in the CO_2-treated group compared with

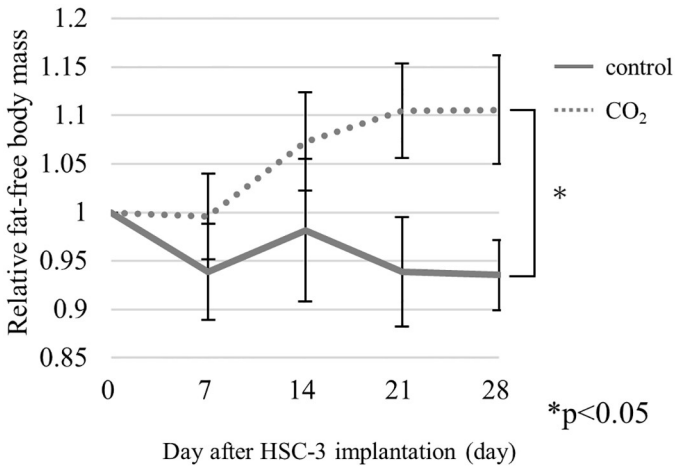

Fig 2. The relative FFM, defined as skeletal muscle mass in the control group (n = 7) and CO_2-treated group (n = 7) (*P<0.05). At the end of the experiment, FFM (average ± standard deviation) of the control group was 0.94 ± 0.10, and that of the CO_2-treated group was 1.11± 0.15.

https://doi.org/10.1371/journal.pone.0302194.g002

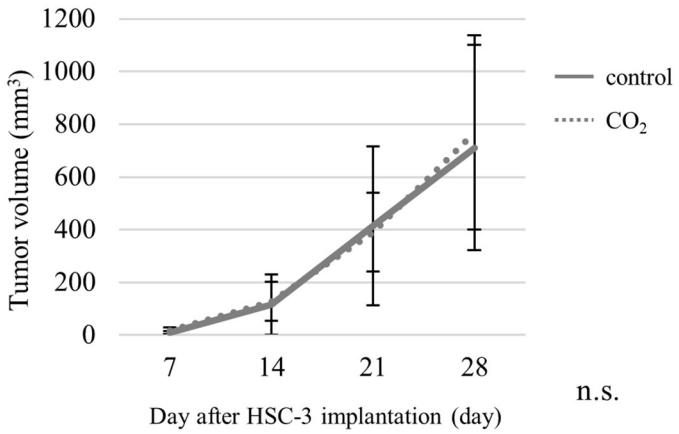

Fig 3. Tumor volumes in the control group (n = 7) and CO_2-treated group (n = 7).

https://doi.org/10.1371/journal.pone.0302194.g003

the control group, consistent with the quantitative real-time PCR results (Figs 5 and 6). MAFbx expression (± standard deviation) in the control group was 0.95±0.04, and that in the CO_2-treated group was 0.17±0.04. MuRF-1 expression in the control group was 0.98±0.02, and that in the CO_2-treated group was 0.26±0.07. UCP2 expression in the control group was 0.93±0.04 and that in the CO_2-treated group was 0.20±0.11. UCP3 expression in the control group was 0.91±0.07, and that in the CO_2-treated group was 0.16±0.06.

5. Cross-sectional area of muscle

Skeletal muscle atrophy caused a decrease in the myofiber area of the muscle tissue. At the end of the experiment, the relative cross-sectional area of the muscle (mean ± standard deviation) of the control group was 1.00 ± 0.17, and that of the CO_2-treated group was 1.75 ± 0.21. Furthermore, the relative cross-sectional area of the muscle of the CO_2-treated group was significantly larger than that of the control group (Figs 7 and 8).

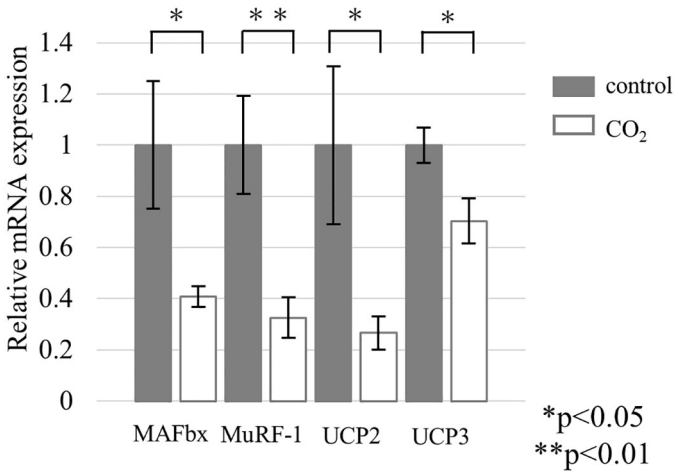

Fig 4. Relative mRNA expression in the control group (n = 7) and CO_2-treated group (n = 7) (*P<0.05, **P<0.01).

https://doi.org/10.1371/journal.pone.0302194.g004

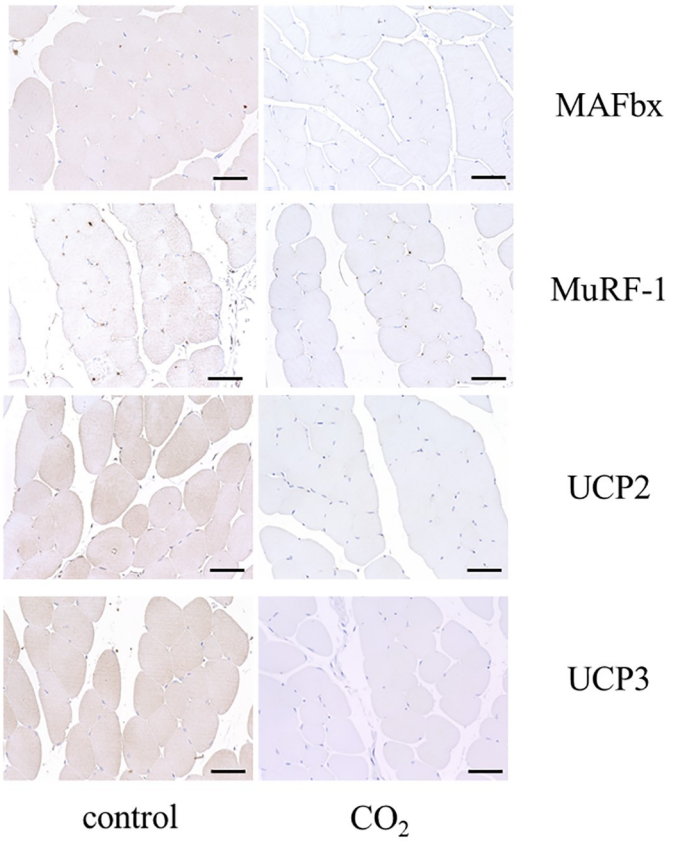

Fig 5. Immunohistochemical staining for MAFbx, MuRF-1, UCP2, and UCP3 in the control group and CO_2-treated group. The representative images are shown at ×400 magnification. Scale bar = 50 μm.

https://doi.org/10.1371/journal.pone.0302194.g005

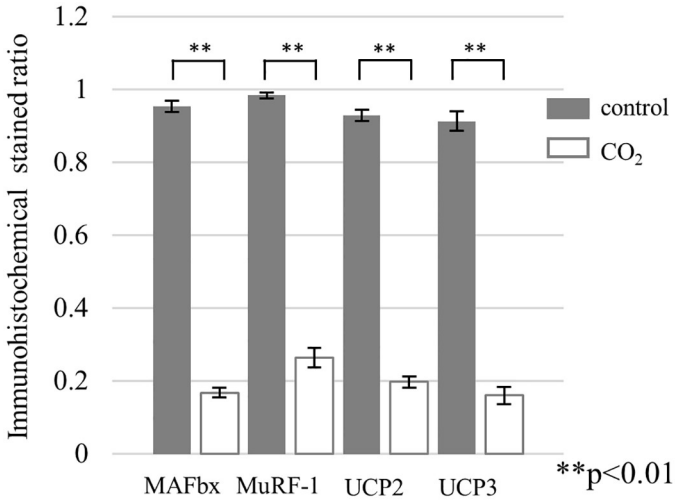

Fig 6. Immunohistochemical staining ratio for MAFbx, MuRF-1, UCP2, and UCP3 in the control group (n = 7) and CO_2-treated group (n = 7) (P<0.01).** MAFbx expression (± standard deviation) in the control group was 0.95 ±0.04, and that in the CO2-treated group was 0.17±0.04. MuRF-1 expression in the control group was 0.98±0.02, and that in the CO2-treated group was 0.26±0.07. UCP2 expression in the control group was 0.93±0.04 and that in the CO2-treated group was 0.20±0.11. UCP3 expression in the control group was 0.91±0.07, and that in the CO2-treated group was 0.16±0.06.

https://doi.org/10.1371/journal.pone.0302194.g006

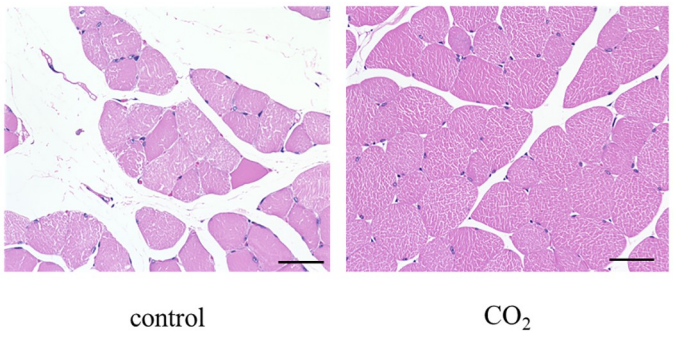

Fig 7. H&E staining of quadriceps muscle in the control group and CO_2-treated group. The representive images are shown at ×400 magnification. Scale bar = 50μm.

https://doi.org/10.1371/journal.pone.0302194.g007

Discussion

Cachexia is a term that has been used for a long time to describe a state of wasting due to poor nutrition [1, 2]. Fearon et al. proposed a cancer-specific definition of cachexia in 2011 [1]. In this definition, cancer cachexia is loss of skeletal muscle mass through a progressively catabolic state.

Previous studies have attempted approaches including nutritional therapy, exercise therapy, and pharmacotherapy. However, these have not yet been established as definitive treatments for cancer, including head and neck cancers [4, 29–31]. Grande AJ et al. examined exercise therapy in patients with lean body masses in a study of cancer cachexia in adults, similar to our study. However, they concluded that the results were highly unclear. Because many cancer patients have impaired cardiac function or advanced anemia, these limitations could make it difficult for them to undertake appropriate exercise [30]. Furthermore, cancer cachexia is associated with increased side effects of chemotherapy and radiotherapy and increased complications associated with surgery, as well as a worse prognosis, including in head and neck cancer [3, 32].

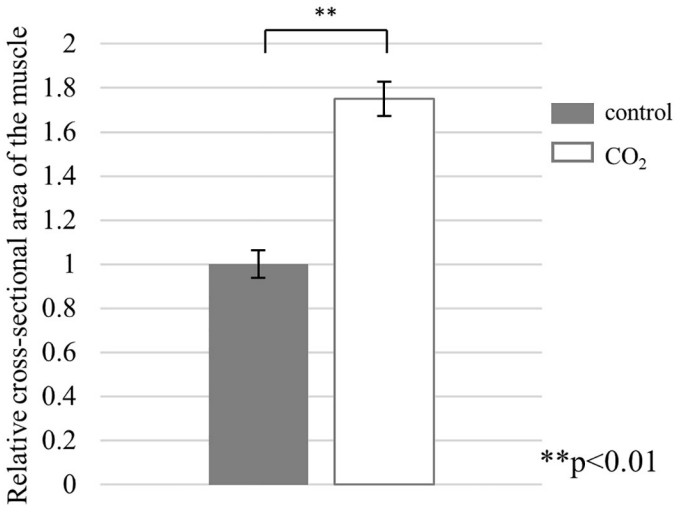

Fig 8. The relative cross-sectional area of quadriceps muscle in the control group (n = 7) and CO_2-treated group (n = 7) (P<0.01).** The relative cross-sectional area of the muscle (mean ± standard deviation) of the control group was 1.00 ± 0.17, and that of CO_2-treated group was 1.75 ± 0.21.

https://doi.org/10.1371/journal.pone.0302194.g008

CO_2 therapy has been indicated for various diseases such as heart disease and skin conditions. The therapeutic effects of CO_2 are mediated by an increase in blood flow and microcirculation, nitric oxide-dependent neocapillary formation, and increased partial pressure of oxygen in the local tissue, known as the Bohr effect. We have developed a new transcutaneous CO_2 application system using 100% CO_2 gas and a transdermal CO_2 absorption-enhancing hydrogel [16]. This treatment has been used previously in several animal models, and it can increase local blood flow, prevent muscle atrophy and contraction, and recover muscle damage [18–23]. Oe et al. demonstrated similar changes to those that occur within muscles when aerobic exercise is performed [23]. And we have shown that the transcutaneous application of CO_2 to the human neck and lower extremities can improve blood flow [17]. However, the effect of transcutaneous application of CO_2 on cancer-related skeletal muscle atrophy is still unknown.

Skeletal muscle mass is maintained by a balance between the processes of protein synthesis and proteolysis. In cancer cachexia, this balance shifts to a catabolic state, leading to skeletal muscle atrophy [6]. It is known that many intracellular signals are activated by inflammatory mediators (such as cytokines) and tumor-derived factors (such as proteolysis-inducing factors). These factors activate forkhead family transcription factors, which enable transcription of genes encoding ubiquitin ligases [5]. The ubiquitin–proteasome pathway is known to be the primary proteolytic pathway in cancer cachexia and is induced by the E3 ubiquitin ligases [8, 9]. MAFbx and MuRF-1 are known E3 ubiquitin ligases specific to skeletal muscle and are often used as indicators of the muscle atrophy [6–11]. Proteasomes recognize and degrade ubiquitinated proteins. The expression of MAFbx and MuRF-1 are also known to be upregulated in skeletal muscle, as shown in various animal carcinoma models [8–11].

UCPs are identified as carriers of proton ions between the mitochondrial inner membrane and the mitochondrial matrix. When UCPs are increased, ATP synthesis is inhibited and is dissipated as heat. It is known that UCP2 is expressed in all tissues, including skeletal muscle, and UCP3 expression is present in skeletal and cardiac muscle [12]. In the skeletal muscle of a cancer-bearing animal model, it has been suggested that a decrease in mitochondrial ATP synthesis might occur due to the upregulation of UCPs [15]. In fact, Busquets et al. and Constantinou et al. demonstrated that a cancer-bearing rat model exhibited significantly more pronounced skeletal muscle atrophy compared with the control group rats, and the expression of UCP2 and UCP3 in skeletal muscles was significantly upregulated [13, 14]. Based on the above, in cancer cachexia, the activation of the ubiquitin–proteasome pathway and UCPs results in muscle atrophy. Additionally, the upregulation of UCPs could potentially lead to the downregulation of mitochondrial ATP synthesis.

In this study, we applied the transcutaneous application of CO_2 to cancer-related skeletal muscle atrophy in vivo. We hypothesized that if the skeletal muscle atrophy improves, these four factors would be downregulated in skeletal muscle in the CO_2-treated group. Skeletal muscle mass significantly differed between the control and CO_2-treated group in the measurement of fat-free body mass by bioimpedance spectroscopy. Skeletal muscle atrophy was significantly suppressed in the cross-sectional area analysis of muscle in the CO_2-treated group. The mRNA expression of *MAFbx*, *MuRF-1*, *UCP2*, and *UCP3* was also predominantly downregulated in the CO_2-treated group. Additionally, the expression of these four factors in the CO_2-treated group was lower compared with that in control group by IHC staining. This indicated that the transcutaneous application of CO_2 to skeletal muscle suppresses muscle atrophy through the downregulation of the ubiquitin–proteasome pathway and UCPs. This result is consistent with previous reports [7–11]. Furthermore, it was demonstrated that inhibiting the ubiquitin–proteasome pathway through the transcutaneous application of CO_2 can suppress catabolism within the muscle tissue. It was also demonstrated that UCP2 and UCP3 expression can be decreased in skeletal muscle atrophy, suggesting a increase in ATP synthesis within the

mitochondria, consistent with previous reports [13, 15]. Therefore, this mechanism may be considered to bring about an improvement in muscle atrophy through the enhancement of the expression of the four factors and the activation of the mitochondria pathway induced by CO_2. However, t it has been reported that the expression of UCP3 was significantly increased, but UCP2 expression was not significantly increased in the skeletal muscle of cancer-bearing mice [14, 15, 33]. This result differs from those in our study. Furthermore, this study has some limitations. First, it is difficult to conduct experiments under pair-feeding conditions at our institute. Even if we could conduct experiments under pair-feeding conditions and maintain the same conditions such as food consumption, liquid consumption, and activity, the effects of cancer cachexia might vary widely among individuals. Second, we demonstrated that transcutaneous application of CO_2 to skeletal muscle increased the number of mitochondria [18], but it is unclear whether this increase leads to elevated ATP synthesis. However, Vohwinkel et al. and Ceco et al. demonstrated that the potential biological effects of CO_2 might also be related to cancer cachexia [34, 35], but in this study, the relationship was unclear. Third, we should focus on myogenesis-related factors as well as muscle atrophy factors in the future.

Conclusions

In conclusion, we suggested that transcutaneous CO_2 application to skeletal muscle suppresses the skeletal muscle atrophy of oral squamous cell cancer-bearing mice. These effects are thought to be due to inhibition of the ubiquitin–proteasome pathway in skeletal muscle, and the promotion of ATP synthesis might be related also. Due to its affordability and non-invasive nature, the CO_2 treatment is easily applicable to humans. Therefore, it could be a preferred treatment option for patients with cancer cachexia. Additional research should be conducted to validate our findings.

Supporting information

S1 Data.
(XLSX)

Acknowledgments

We thank for Nobuyuki Endo at KEYENCE for his expert technical assistance. We also thank H. Nikki March, PhD, from Edanz (https://jp.edanz.com/ac) for editing a draft of this manuscript.

Author Contributions

Conceptualization: Aki Sasaki, Daisuke Takeda, Takumi Hasegawa.

Data curation: Aki Sasaki, Daisuke Takeda, Hotaka Kawai.

Formal analysis: Aki Sasaki, Daisuke Takeda, Hotaka Kawai.

Investigation: Yoshiaki Tadokoro, Aki Murakami, Nanae Yatagai, Satomi Arimoto.

Supervision: Hitoshi Nagatsuka, Masaya Akashi.

Validation: Aki Sasaki, Daisuke Takeda.

Writing – original draft: Aki Sasaki, Daisuke Takeda.

Writing – review & editing: Takumi Hasegawa.

References

1. Fearon K, Strasser F, Anker SD, Bosaeus I, Bruera E, Fainsinger RL, et al. Definition and classification of cancer cachexia: an international consensus. Lancet Oncol. 2011 May; 12(5):489–95. https://doi.org/10.1016/S1470-2045(10)70218-7 PMID: 21296615
2. Evans WJ, Morley JE, Argilés J, Bales C, Baracos V, Guttridge D, et al. Cachexia: a new definition. Clin Nutr. 2008 Dec; 27(6):793–9. https://doi.org/10.1016/j.clnu.2008.06.013 PMID: 18718696
3. Nishikawa H, Goto M, Fukunishi S, Asai A, Nishiguchi S, Higuchi K. Cancer Cachexia: Its Mechanism and Clinical Significance. Int J Mol Sci. 2021 Aug 6; 22(16):8491. https://doi.org/10.3390/ijms22168491 PMID: 34445197
4. Roeland EJ, Bohlke K, Baracos VE, Bruera E, Del Fabbro E, Dixon S, et al. Management of Cancer Cachexia: ASCO Guideline. J Clin Oncol. 2020 Jul 20; 38(21):2438–2453. https://doi.org/10.1200/JCO.20.00611 PMID: 32432946
5. Argilés JM, Busquets S, Stemmler B, López-Soriano FJ. Cancer cachexia: understanding the molecular basis. Nat Rev Cancer. 2014 Nov; 14(11):754–62. https://doi.org/10.1038/nrc3829 PMID: 25291291
6. Sukari A, Muqbil I, Mohammad RM, Philip PA, Azmi AS. F-BOX proteins in cancer cachexia and muscle wasting: Emerging regulators and therapeutic opportunities. Semin Cancer Biol. 2016 Feb; 36:95–104. https://doi.org/10.1016/j.semcancer.2016.01.002 PMID: 26804424
7. Bodine SC, Latres E, Baumhueter S, Lai VK, Nunez L, Clarke BA, et al. Identification of ubiquitin ligases required for skeletal muscle atrophy. Science. 2001 Nov 23; 294(5547):1704–8. https://doi.org/10.1126/science.1065874 PMID: 11679633
8. Chen MC., Hsu W., Hwang P., Chen Y., Chou T. Combined administration of fucoidan ameliorates tumor and chemotherapy-induced skeletal muscle atrophy in bladder cancer-bearing mice. Oncotarget. 2016; 7: 51608–51618. https://doi.org/10.18632/oncotarget.9958 PMID: 27323407
9. Rom O, Reznick AZ. The role of E3 ubiquitin-ligases MuRF-1 and MAFbx in loss of skeletal muscle mass. Free Radic Biol Med. 2016 Sep; 98:218–230. https://doi.org/10.1016/j.freeradbiomed.2015.12.031 PMID: 26738803
10. Julienne CM, Dumas JF, Goupille C, Pinault M, Berri C, Collin A, et al. Cancer cachexia is associated with a decrease in skeletal muscle mitochondrial oxidative capacities without alteration of ATP production efficiency. J Cachexia Sarcopenia Muscle. 2012 Dec; 3(4):265–75. https://doi.org/10.1007/s13539-012-0071-9 PMID: 22648737
11. Costelli P, Muscaritoli M, Bossola M, Penna F, Reffo P, Bonetto A, et al. IGF-1 is downregulated in experimental cancer cachexia. Am J Physiol Regul Integr Comp Physiol. 2006 Sep; 291(3):R674–83. https://doi.org/10.1152/ajpregu.00104.2006 PMID: 16614058
12. Joshi M, Patel BM. Unveiling the Role of the Proton Gateway, Uncoupling Proteins (UCPs), in Cancer Cachexia. Cancers (Basel). 2023 Feb 23; 15(5):1407. https://doi.org/10.3390/cancers15051407 PMID: 36900198
13. Busquets S, Almendro V, Barreiro E, Figueras M, Argilés JM, López-Soriano FJ. Activation of UCPs gene expression in skeletal muscle can be independent on both circulating fatty acids and food intake. Involvement of ROS in a model of mouse cancer cachexia. FEBS Lett. 2005 Jan 31; 579(3):717–22. https://doi.org/10.1016/j.febslet.2004.12.050 PMID: 15670834
14. Constantinou C, Fontes de Oliveira CC, Mintzopoulos D, Busquets S, He J, Kesarwani M, et al. Nuclear magnetic resonance in conjunction with functional genomics suggests mitochondrial dysfunction in a murine model of cancer cachexia. Int J Mol Med. 2011 Jan; 27(1):15–24. https://doi.org/10.3892/ijmm.2010.557 PMID: 21069263
15. Tzika AA, Fontes-Oliveira CC, Shestov AA, Constantinou C, Psychogios N, Righi V, et al. Skeletal muscle mitochondrial uncoupling in a murine cancer cachexia model. Int J Oncol. 2013 Sep; 43(3):886–94. https://doi.org/10.3892/ijo.2013.1998 PMID: 23817738
16. Sakai Y, Miwa M, Oe K, Ueha T, Koh A, Niikura T, et al. A novel system for transcutaneous application of carbon dioxide causing an "artificial Bohr effect" in the human body. PLoS One. 2011; 6(9):e24137. https://doi.org/10.1371/journal.pone.0024137 PMID: 21931656
17. Yatagai N, Hasegawa T, Kyotani K, Noda T, Amano R, Saito I, et al. Exploratory clinical trial to evaluate the efficacy and safety of carbon dioxide paste in healthy people. Medicine (Baltimore). 2022 Jul 22; 101(29):e29511. https://doi.org/10.1097/MD.0000000000029511 PMID: 35866800
18. Inoue M, Sakai Y, Oe K, Ueha T, Koga T, Nishimoto H, et al. Transcutaneous carbon dioxide application inhibits muscle atrophy after fracture in rats. J Orthop Sci. 2020 Mar; 25(2):338–343. https://doi.org/10.1016/j.jos.2019.03.024 PMID: 31031109
19. Hirota J, Hasegawa T, Inui A, Takeda D, Amano-Iga R, Yatagai N, et al. Local application of a transcutaneous carbon dioxide paste prevents excessive scarring and promotes muscle regeneration in a

bupivacaine-induced rat model of muscle injury. Int Wound J. 2023 Apr; 20(4):1151–1159. https://doi.org/10.1111/iwj.13974 PMID: 36250918

20. Akahane S, Sakai Y, Ueha T, Nishimoto H, Inoue M, Niikura T, et al. Transcutaneous carbon dioxide application accelerates muscle injury repair in rat models. Int Orthop. 2017 May; 41(5):1007–1015. https://doi.org/10.1007/s00264-017-3417-2 PMID: 28210805

21. Nishimoto H, Inui A, Ueha T, Inoue M, Akahane S, Harada R, et al. Transcutaneous carbon dioxide application with hydrogel prevents muscle atrophy in a rat sciatic nerve crush model. J Orthop Res. 2018 Jun; 36(6):1653–1658. https://doi.org/10.1002/jor.23817 PMID: 29193246

22. Inoue S, Moriyama H, Wakimoto Y, Li C, Hatakeyama J, Wakigawa T, et al. Transcutaneous application of carbon dioxide improves contractures after immobilization of rat knee joint. Phys Ther Res. 2020 Jul 22; 23(2):113–122. https://doi.org/10.1298/ptr.E10023 PMID: 33489648

23. Oe K, Ueha T, Sakai Y, Niikura T, Lee SY, Koh A, et al. The effect of transcutaneous application of carbon dioxide (CO) on skeletal muscle. Biochem Biophys Res Commun. 2011 Apr 1; 407(1):148–52.

24. Takeda D, Hasegawa T, Ueha T, Imai Y, Sakakibara A, Minoda M, et al. Transcutaneous carbon dioxide induces mitochondrial apoptosis and suppresses metastasis of oral squamous cell carcinoma in vivo. PLoS One. 2014 Jul 2; 9(7):e100530. https://doi.org/10.1371/journal.pone.0100530 PMID: 24988190

25. Zhang J, Zheng J, Chen H, Li X, Ye C, Zhang F, et al. Curcumin Targeting NF-κB/Ubiquitin-Proteasome-System Axis Ameliorates Muscle Atrophy in Triple-Negative Breast Cancer Cachexia Mice. Mediators Inflamm. 2022 Jan 29; 2022:2567150.

26. Meng X, Huang Z, Inoue A, Wang H, Wan Y, Yue X, et al. Cathepsin K activity controls cachexia-induced muscle atrophy via the modulation of IRS1 ubiquitination. J Cachexia Sarcopenia Muscle. 2022 Apr; 13(2):1197–1209. https://doi.org/10.1002/jcsm.12919 PMID: 35098692

27. Liu Z, Xiong J, Gao S, Zhu MX, Sun K, Li M, et al. Ameliorating cancer cachexia by inhibiting cancer cell release of Hsp70 and Hsp90 with omeprazole. J Cachexia Sarcopenia Muscle. 2022 Feb; 13(1):636–647. https://doi.org/10.1002/jcsm.12851 PMID: 34729960

28. Lai KC, Hong ZX, Hsieh JG, Lee HJ, Yang MH, Hsieh CH, et al. IFIT2-depleted metastatic oral squamous cell carcinoma cells induce muscle atrophy and cancer cachexia in mice. J Cachexia Sarcopenia Muscle. 2022 Apr; 13(2):1314–1328. https://doi.org/10.1002/jcsm.12943 PMID: 35170238

29. Tanaka K, Nakamura S, Narimatsu H. Nutritional Approach to Cancer Cachexia: A Proposal for Dietitians. Nutrients. 2022 Jan 14; 14(2):345. https://doi.org/10.3390/nu14020345 PMID: 35057531

30. Grande AJ, Silva V, Sawaris Neto L, Teixeira Basmage JP, Peccin MS, Maddocks M. Exercise for cancer cachexia in adults. Cochrane Database Syst Rev. 2021 Mar 18; 3(3):CD010804. https://doi.org/10.1002/14651858.CD010804.pub3 PMID: 33735441

31. Belda-Iniesta C, de Castro Carpeno J, Fresno Vara JA, Cejas Guerrero P, Casado Saenz E, Espinosa Arranz E, et al. Eicosapentaenoic acid as a targeted therapy for cancer cachexia. J Clin Oncol. 2003 Dec 15; 21(24):4657–8; author reply 4658. https://doi.org/10.1200/JCO.2003.99.154 PMID: 14673061

32. Caillet P, Liuu E, Raynaud Simon A, Bonnefoy M, Guerin O, Berrut G, et al. Association between cachexia, chemotherapy and outcomes in older cancer patients: A systematic review. Clin Nutr. 2017 Dec; 36(6):1473–1482. https://doi.org/10.1016/j.clnu.2016.12.003 PMID: 28017447

33. Collins P, Bing C, McCulloch P, Williams G. Muscle UCP-3 mRNA levels are elevated in weight loss associated with gastrointestinal adenocarcinoma in humans. Br J Cancer. 2002 Feb 1; 86(3):372–5. https://doi.org/10.1038/sj.bjc.6600074 PMID: 11875702

34. Vohwinkel CU, Lecuona E, Sun H, Sommer N, Vadász I, Chandel NS, et al. Elevated CO(2) levels cause mitochondrial dysfunction and impair cell proliferation. J Biol Chem. 2011 Oct 28; 286(43):37067–76. https://doi.org/10.1074/jbc.M111.290056 PMID: 21903582

35. Ceco E, Celli D, Weinberg S, Shigemura M, Welch LC, Volpe L, et al. Elevated CO2 Levels Delay Skeletal Muscle Repair by Increasing Fatty Acid Oxidation. Front Physiol. 2021 Jan 21; 11:630910. https://doi.org/10.3389/fphys.2020.630910 PMID: 33551852